

# **Lipid Bilayer Composition Influences the Activity of the Antimicrobial Peptide Dermcidin Channel**

Chen Song,<sup>1,2,3,\*</sup> Bert L. de Groot,<sup>4</sup> and Mark S. P. Sansom<sup>3</sup>

<sup>1</sup>*Center of Quantitative Biology, Academy for Advanced Interdisciplinary Studies, Peking University, Beijing, China*

<sup>2</sup>*Peking-Tsinghua Center for Life Sciences, Peking University, Beijing, China*

<sup>3</sup>*Department of Biochemistry, University of Oxford, Oxford, U.K.*

<sup>4</sup>*Department of Theoretical and Computational Biophysics, Max-Planck Institute for Biophysical Chemistry, Göttingen, Germany*

\*Correspondence: c.song@pku.edu.cn

**Running Title:** Lipid Bilayer Affects Dermcidin Activity

## Abstract

Antimicrobial peptides carry great potential as new antibiotics against ‘superbugs’. Dermcidin, a broad-spectrum antimicrobial peptide in human sweat, has been recently crystallized in its oligomeric state and showed channel-like properties. In the present work, we performed multi-scale molecular dynamics simulations to study how the membrane composition influences the behavior of a transmembrane pore formed by the dermcidin oligomer, in the hope of revealing the origin of the membrane selectivity of this antimicrobial peptide towards bacteria. Our results indicate that bilayers composed of various lipids (DMPC, DPPC and DSPC) with different thicknesses result in different orientations of the dermcidin oligomer when embedded in lipid bilayers. The thicker the bilayer, the less tilted the channel. Cholesterol makes the bilayers more rigid and thicker, which also affects the orientation of the channel. Furthermore, we observed that the predicted conductance of the channel from computational electrophysiology simulations is related to its orientation in the lipid bilayer: the larger the tilt, the larger the conductance. Our results indicate that the membrane composition has a significant influence on the activity of the dermcidin channel, with thicker, cholesterol-rich membranes showing lower conductance than thinner membranes.

## Introduction

Due to the overuse and misuse of existing antibiotics as well as the slow development of new antibiotics, many pathogenic species of bacteria are developing resistance to existing antibiotics, which has become one of the world's most pressing public health concerns (1). Antimicrobial peptides (AMPs), which widely exist in various forms of lives from plant to mammals, exhibit great potential as a new generation of antibiotics. Many kinds of AMPs kill bacteria by interacting with their membranes rather than with specific proteins, and thereby make it harder for bacteria to develop resistance (2, 3). Therefore, it is of great interest to understand how AMPs interact with membranes, with a long-term goal of understanding the detailed mechanisms of action of AMPs enabling development of potential new antibiotics.

The various types of AMPs differ in their sequence, length, structure, net charge and other properties (4). It has been proposed that some AMPs function as metabolic inhibitors, whereas others can increase the permeability of membranes by various mechanisms (3). Three permeation models have dominated discussion of AMPs: the barrel-stave, toroidal, and carpet models (3). It is likely the detailed pore-forming mechanism varies between different AMPs. A number of computational studies have attempted to address possible mechanisms of pore formation and/or interaction with membranes (5–13). Such studies can reveal aspects of the underlying mode(s) of action of AMPs and thereby provide a guide for design of novel antibiotics (2, 14–17).

Among recently discovered AMPs, Dermcidin (DCD) was initially discovered in human sweat in 2001 and found to have broad-spectrum antimicrobial and antifungal activities under a wide range of conditions (18). Significantly, deficiency of DCD in the sweat of patients with atopic dermatitis correlates with an impaired resistance to infection of human skin (19). There have been several studies performed to investigate its functional mechanism (19–25). DCD is a 47-residue peptide, the monomeric structure of which was determined by NMR and shown to be a kinked  $\alpha$ -helix (26). The DCD monomer is negatively charged, which is unusual for an AMP, many of which are cationic (3, 27) in order to facilitate peptide/lipid interactions. Based on structure-activity studies of DCD-1L it was proposed to form oligomeric complexes, stabilized by  $\text{Zn}^{2+}$  ions, which form ion permeable pores i.e. channels in the bacterial membrane (18, 28).

A crystal structure of a channel-like helix-bundle oligomer of DCD in combination with molecular dynamics (MD) simulations and ion channel current measurements was used to propose a detailed mechanism for the action of this unusual AMP (28). It was suggested that pore formation by DCD involves the divalent ion  $\text{Zn}^{2+}$  such that the oligomeric complex is neutral. This oligomeric structure can form a stable pore when embedded in a lipid bilayer in accord with the barrel-stave model, and the pore shows high water and ion permeability. This pore-forming mechanism may therefore explain how DCD kills bacteria (28).

In order to both understand and to potentially engineer selectivity of AMPs, it is important to understand how membrane lipid composition (which differs profoundly between bacterial and mammalian cells) influences the behavior of DCD. In the current study we performed multi-scale MD simulations to study the effect of the membrane lipid composition on the orientation and predicted conduction properties of DCD when embedded in various lipid bilayers. The orientation of DCD relative to the bilayer is shown to be correlated with the lipid bilayer thickness: the thicker the bilayer, the less the tilt of the channel assembly relative to the bilayer plane. The conductance of the channel exhibits a correlation with the tilt of DCD such that more tilted channels exhibit a larger conductance. This suggests that the biological activity of the DCD pore will be strongly influenced by the nature of the membrane within which the DCD oligomer is embedded.

## **Methods**

### **Selection of the Simulation Systems**

We took the crystal structure of the hexameric DCD pore (PDB ID 2YMK) as the initial structure for our MD simulations. To study the effect of membrane thickness and composition on the DCD activity, we selected three kinds of lipids with different lengths, namely DMPC, DPPC and DSPC, which have 14, 16, and 18 carbon atoms in the fatty acid chains respectively. Moreover, we added cholesterol into some of the simulation systems to study its influence for a given lipid type. Therefore, we studied the following systems: DCD in DMPC, DCD in DPPC and DCD in DSPC bilayers, with 0%, 20%, and 40% cholesterol in the each of the respective lipid bilayers.

## Coarse Grain Simulations

To investigate the orientation of the DCD oligomer on various lipid bilayers, we performed coarse grain (CG) MD simulations (29) to study the self-assembly processes of the DCD oligomer into lipid bilayers. Initially, the DCD oligomer was positioned along the z-axis or perpendicular to the z-axis, and was surrounded by randomly positioned lipids and water molecules (and cholesterol as well for some cases) in a simulation box of  $120 \times 120 \times 80 \text{ \AA}^3$ , which was sandwiched into two extra water layers with the thickness of  $20 \text{ \AA}$  along the z-axis. As a consequence, the initial simulation system was a box of  $120 \times 120 \times 120 \text{ \AA}^3$  as shown in Fig. 1A-B. In all the CG simulations, we included the six  $\text{Zn}^{2+}$  ions within the DCD hexamer, as these have been shown to be important for the stability of the oligomeric structure (28). There are not well-established  $\text{Zn}^{2+}$  parameters in the Martini force field, so in the CG we used generic divalent cation parameters represented by  $\text{Ca}^{2+}$ . We consider this strategy to be reasonable as an elastic network was applied to the DCD- $\text{Zn}^{2+}$  complex as a whole, thus ensuring its conformational stability.

Then the system was heated up to 345 K, all the molecules in the simulations box being allowed to move freely. Within 200 ns, the system was able to reach a well-equilibrated condition, where the DCD oligomer self-inserted into a well-shaped lipid bilayer which was sandwiched by extra- and intra-water layers representing the extra- and intra-cellular environment (Fig. 1C), or in rare cases the oligomer was found to be partly embedded into the lipid bilayer and partly exposed to water, with the pore axis parallel to the bilayer surface as shown in Fig. 1D. The temperature of 345 K was chosen to make sure all the lipids will stay in the fluid phase.

For the CG simulations, we used Gromacs4.6 (30) to perform the MD simulations with the Martini force field (29, 31). A time step of 20 fs was adopted. We used the Berendsen barostat (32) and the v-rescale thermostat (33), with a time constant of 1.0 ps for both. The short range van der Waals (vdW) and electrostatic interactions were calculated with a cut-off of  $11 \text{ \AA}$ . The electrostatic interactions were calculated with the "Reaction Field" method. The dielectric constant was set to be 15. More details about the self-assembly CG simulations can also be found in a recently established automated method (34).

## Atomistic Computational Electrophysiology Simulations

Atomistic computational electrophysiology (CE) simulation is a recently developed method, which is highly suitable for the study of ion conduction properties of channels or pores (35, 36). In such a simulation, we set up a double layer system, where the simulation box is divided into three segments by two lipid bilayers. Effectively, there are only two water compartments named W1 and W2 in the simulation system, as the top and lower water sections are actually treated as continuous with one another in the simulations, due to the existence of periodic boundary conditions, as shown in Fig. 1E. Different numbers of ions can be put into the two water compartments, which can generate a transmembrane ion gradient and transmembrane potential due to the imbalance of the ion distribution. By adjusting the ion number difference in the two water compartments, we can apply a desired transmembrane potential to the simulation system.

The DCD hexamer and the six  $\text{Zn}^{2+}$  ions within the channel were extracted from PDB 2YMK to build the all-atom simulation system. The atomistic MD simulations were performed with Gromacs4.6 (30) and the CHARMM36 force field (37). Using g\_membed (38), we first embedded the DCD oligomer into a lipid bilayer built with CHARMM-GUI (39), and further solvated the system by water molecules and a certain number of ions to have an ion (NaCl) concentration of 0.15 M. The resulting system is overall neutral. We adopted a time step of 2 fs. The semi-isotropic NPT barostat was applied with the Parrinello-Rahman method at 1 bar with a coupling time constant of 1.0 ps (40, 41), and the thermostat was applied with the Nose-Hoover method at 345 K with a coupling time constant of 0.5 ps (42, 43). The short range electrostatic interaction cut off was set to be 14 Å, and the particle mesh ewald (PME) method was utilized for calculating long range coulomb interactions (44, 45). The vdW interactions were cut off at 12 Å, and turned off smoothly from 8 to 12 Å with the ‘shift’ method.

The single layer system was firstly equilibrated for 500 ns, until the channel finds its most stable orientation in the lipid bilayer. The resulting system has a size of around  $80 \times 80 \times 110 \text{ Å}^3$ . Then the single-layer system was duplicated along the  $z$  direction. We set the number of  $\text{Cl}^-$  to be 45 and 39, and the number of  $\text{Na}^+$  to be 39 and 45 in W1 and W2 respectively, which lead to a transmembrane potential of about 300-450 mV. Then, we ran multiple 200-ns CE simulations for each system. From these production CE simulations, we were able to

observe continuous ion permeation along the DCD oligomer. In the end, we calculated the average transmembrane potential and the current during the simulation time (divided into 200-ns segments), and thereby obtained the conductance of the channel. We performed 200-ns atomistic CE simulations for DCD in DMPC, DPPC, DSPC and DMPC+cholesterol bilayers. All the simulations are summarized in Tab. S4.

## Calculation of the Channel Conductance

After finishing the CE simulations, we analyzed the transmembrane potential, which was generated from the charge imbalance  $\Delta q$  between the two water compartments. Only the charge distribution perpendicular to the membrane is relevant for calculating the potential drop  $\Delta U$ , so we integrated twice over the charge distribution with intervals along  $z$  (the bilayer normal direction) to obtain the transmembrane potential, by using the implementation of the Poisson equation ( $\nabla^2 U = -\rho/\epsilon$ ) in the GROMACS `g_potential` tool. Then we counted the number of ions that permeated through the channel in the 200-ns MD trajectories, with which we calculated the current with the equation:  $I = Q/t$ , where  $Q = e \times (num_{Na+} + num_{Cl-})$  was the charge that passed through the channel and  $t$  was the simulation time. With  $\Delta U$  and  $I$  known, the conductance was simply calculated with the equation:  $C = I/\Delta U$ . The above calculation was performed for each 200-ns CE simulation.

## Results

### The orientation of the DCD oligomer is membrane dependent

In the CG MD simulations, the lipids (and cholesterol) self-assembled into a bilayer around the DCD oligomer. Most of the self-assembly processes were completed within 200 ns, as indicated by a well-defined lipid bilayer forming around the DCD oligomer (Fig. 1C,D) and the tilt angle reaching a stable value (Fig. 2). If the DCD oligomer was initially parallel to the  $z$ -axis (red plot, initial tilt angle  $0^\circ$ ), its final orientation was mostly embedded and tilted in the self-assembled lipid bilayer. The exceptions were two out of ten simulations with 80%DMPC:20%Chol, and one out of ten simulations with 60%DMPC:40%Chol, where the DCD was only partially embedded into the bilayer and its axis is parallel to the bilayer surface. If the DCD oligomer was

initially normal to the z-axis (blue plot, initial tilt angle  $90^\circ$ ), the final orientation can be either embedded and tilted in the lipid bilayer, or partially embedded into the bilayer and parallel to the bilayer surface.

In all of the above simulations, the embedded and tilted orientation was preferred, and the tilt angle was system dependent. We analyzed the tilt angle distribution for all the CG simulations, disregarding the first 200-ns assembly trajectories. We observe two possible orientations, as shown in Fig. 2&S1. The preferred orientation is the DCD oligomer embedded and tilted in the bilayer, and the tilt angle depends on the composition of the bilayer. We found that, the thinner the bilayer, the larger the tilt (Fig. 3). For different types of lipids, the lipids with longer tails (length: DSPC > DPPC > DMPC) form a thicker bilayer, which lead to a less tilted orientation of the DCD oligomer in the bilayer (tilt angle: DSPC < DPPC < DMPC). For the same type of lipids, adding cholesterol results in thicker bilayers, which subsequently lead to a less tilted orientation of the DCD oligomer in the bilayer. The other orientation was the DCD channel axis parallel to the bilayer surface and only partially embedded into the lipid bilayer (Fig. 1D). As this orientation did not eventually lead to a pore formation in the bilayers, we think it is not the functional orientation of the DCD oligomer. Therefore, we focused on the study of the tilted orientation.

## **The orientation of the DCD oligomer from atomistic MD simulations**

Our atomistic simulations show a similar trend to the CG MD simulations. We examined the tilt angle evolution of the DCD oligomer in three different types of lipid bilayers: DMPC, DPPC and DSPC. Initially, the DCD oligomer was embedded into the bilayers with the `g_membed` method (38) and the channel axis was parallel to the z-axis (tilt angle  $0^\circ$ ). During the equilibration period, the channel spontaneously and gradually tilted in all of the three lipid bilayers (Fig. 4a). We also examined the tilt angle evolution in the double-layer computational electrophysiology simulations. As the initial configurations of the double-layer systems were taken from the equilibrated single-layer systems, we found the tilt angles were stable throughout the 200-ns simulations (Fig. 4b), indicating that the single-layer systems were indeed well equilibrated. All these atomistic MD results show that, the tilt angle is dependent on the lipid type: the thicker the bilayer (thickness: DSPC > DPPC > DMPC), the smaller the tilt (tilt angle: DSPC < DPPC < DMPC), as shown in Fig. 4. The tilt angles converged in less than 350 ns for all of the three simulations. The final stable tilt angles are around  $51^\circ$ ,  $41^\circ$  and  $38^\circ$  for DMPC,

DPPC and DSPC respectively, which are close to the results obtained in CG MD simulations. Please refer to the Tab. S1, Tab. S3, and Fig. S1 for a more detailed analysis.

## **The ion conduction through the DCD oligomer is correlated with its orientation**

In our atomistic CE simulations, we counted how many ions permeated through the DCD channel within the simulation time. Together with the average transmembrane potential across the membrane, this allowed us to calculate the predicted conductance of the channel. Also, from the simulation trajectory, we obtained the stable tilt angle of the DCD oligomer in the lipid bilayer. When the conductance values and the tilt angles are plotted in Fig. 5, although there are local variations resulting in a relatively weak correlation coefficient of 0.65, we can see a clear overall trend between the conductance and the tilt angle of the DCD oligomer: the larger the tilt angle, the larger the conductance.

It is also notable that the addition of cholesterol has a significant effect on the DCD tilt angle (black scatters in Fig. 3), as well as on the conductance (Fig. 5). From our simulations, the addition of cholesterol makes the lipid bilayer stiffer and thicker, which in turn leads to a smaller tilt angle and a smaller conductance.

## **Ion permeation path and selectivity**

The majority of the permeating ions are anions. From our analysis, we found that about 90% of the permeating ions were  $\text{Cl}^-$ , indicating the DCD oligomer is anion selective. This is consistent with our previous simulation results in POPE/POPG bilayers, where about 88% permeated ions were anions. Although the DCD peptide is overall negatively charged, there are six  $\text{Zn}^{2+}$  ions forming a complex with the peptides upon oligomerization, which makes the DCD- $\text{Zn}^{2+}$  complex overall neutral. Moreover, the  $\text{Zn}^{2+}$  ions are located near both the end and side openings of the channel, which may facilitate anion permeation. As shown in Fig. S2, the density of  $\text{Cl}^-$  is significant larger than that of  $\text{Na}^+$  at the side entrance of the channel, as well as throughout the interior of the channel. The major permeation pathway was from side openings rather than channel end openings, resulting a zigzag permeation path as we illustrated before (28).

## **The influence of the DCD oligomer on the surrounding lipid bilayer**

The insertion and tilt of the DCD oligomer strongly influences the lipid bilayer properties around it. Unlike most of the membrane proteins which have a symmetric configuration around the z-axis, the tilted DCD oligomer introduces a unique distortion on the lipid bilayer.

As shown in Fig. 6, the tilted DCD oligomer introduces local bending and thinning of the lipid bilayer around it, both in atomistic and CG MD simulations. In the simulation trajectories, we noticed that some lipid head groups around the DCD oligomer were able to move near the center of the lipid bilayer, along the hydrophilic gap on the DCD oligomer outer surface, which effectively thinned the bilayer nearby. It is also notable that the bilayer distortion is not completely identical in atomistic and CG simulations. In fact, the distortion is more pronounced in the atomistic simulations than in CG simulations, which is understandable as the CG models have a smoother surface than atomistic models.

## **Discussion**

It is an important question what causes the selective activity of AMPs against bacteria rather than host cells. Answering this question can not only reveal the detailed function mechanism of AMPs, but also help to develop novel selective antibiotics. As many AMPs execute their function by interacting with membranes, it is a reasonable hypothesis that the composition of membranes may influence of the activity of AMPs, since it has been shown that the membranes of bacteria and human cells have distinct compositions (4, 46). As a first step towards understanding this question, we studied how different types of lipids affect the orientation and conductance of the DCD oligomer when the DCD oligomer is embedded in a lipid bilayer.

Our results confirm that the DCD oligomer indeed prefers to be embedded into the lipid bilayer, which is expected as about two thirds of the outer surface of the DCD oligomer is hydrophobic. When there is a large exposure of the hydrophobic surface to water (i.e. hydrophobic mismatch) the relative free energy of the system will be higher. By being fully embedded in the lipid bilayer, the hydrophobic mismatch is minimized, and the system reaches a more stable state. In such a scenario, changing the lipid tail length, which in turn changes the

bilayer thickness, changes the optimal orientation of the DCD oligomer whilst embedded in the bilayer. As shown in Fig. 3, the stable tilt angle shows a strong correlation with the bilayer thickness in our CG MD simulations: the thicker the bilayer, the less the tilt, as the DCD oligomer can tilt to a smaller extent to minimize the hydrophobic mismatch in a thicker bilayer. We found the same trend in the atomistic MD simulations (Fig. 4 and Tab. S3), although perhaps not surprisingly the tilt angle values do not exactly match those in CG simulations, given the approximations intrinsic in the CG representation. Therefore, the overall trend is the same in both atomistic and CG models: thicker bilayers lead to a less tilted orientation of the DCD oligomer. Also, it was shown that the addition of cholesterol leads to a more rigid and thicker bilayer, and therefore a less tilted orientation of the DCD oligomer in our CG MD simulations. This may lead to a natural hypothesis that the cholesterol may play a role in the selectivity of the AMPs activity, since we already know that cholesterol does not exist in bacteria membranes, but exists in human cells.

It was interesting that an alternative stable orientation of the DCD oligomer was observed in the CG MD simulations, which was not seen in our atomistic simulations. This does not mean there is a discrepancy between the two methods. But rather, it reflects the fact that the CG simulations are able to provide more complex sampling of protein/membrane interactions. CG self-assembly simulations have been proven to be very reliable at studying the orientation of membrane proteins in lipid bilayer due to its high efficiency of sampling, and a web server has been built recently to show what the most likely orientations of integral membrane proteins in lipid bilayers are (<http://memprotmd.bioch.ox.ac.uk/>) (34). Due to this sampling efficiency, CG MD was able to find the alternative orientation of the DCD oligomer: it lies on the bilayer surface, is partially embedded into the bilayer and exposed the hydrophilic gap on the outer surface to the water solution. This way, the oligomer can also reduce the hydrophobic mismatch and find a stable position. We transformed the CG model with this alternative orientation into an atomistic system and ran atomistic MD simulations. The results showed that this alternative orientation is indeed also stable in the atomistic system (Fig. S4). However, this orientation does not fully penetrate the bilayer, and therefore we think it is not a functional pore. We note that the two orientations can interchange within the simulation time scale in our CG MD simulations (Fig. 2), meaning the free energy barrier between the two orientations can be overcome within a reasonable time. The exchange of the two

orientation is rare in our CG simulations though, which is the reason why we did not see the other orientation in our atomistic simulation in which the DCD oligomer was initially embedded in the pre-formed bilayer.

We have previously observed that the DCD oligomer can act as an ion permeable pore when embedded in a lipid bilayer, which is likely its mechanism of action (28). Herein we examined the conductivity of the DCD oligomer by computational electrophysiology simulations in various lipid bilayers in which the peptide adopts different tilt angles. In these simulations, we observed an overall correlation between the predicted conductance and the tilt angle of the DCD channel in various bilayers, from a total of  $\sim 3\text{-}\mu\text{s}$  all-atom CE simulations. We found that the larger the tilt angle, the larger the conductance, as shown in Fig. 5. From our atomistic simulation results, one thing notable is that the addition of cholesterol results in a very broad and scattered distribution of tilt angles and conductance values. The wide distribution of the tilt angle is a bit different from what we see in the CG MD simulations in Fig. S1. We believe this is caused by the fact that the free energy landscape is rougher in atomistic simulations and therefore there are many more meta-stable orientations when cholesterol added. On the one hand, this requires a much longer time to find the most stable and optimal orientation; on the other hand, this gives us an opportunity to study the correlation between the conductance and the tilt angle for a given membrane composition, as we have enough time to measure the conductance for a meta-stable orientation before it spontaneously evolved to the next state and no external restraint is required. Interestingly, the six simulations of the DCD oligomer in the DMPC and cholesterol mixture bilayer showed the same trend as well: the larger the tilt angle, the larger the conductance (black circles in Fig. 5). Taken together, we found an overall correlation between the conductance and the tilt of the channel with a correlation coefficient of 0.65.

We also note that we do not expect this trend to hold at very large tilt angles. In our simulations, we have only seen tilt angles from around  $20^\circ$  to  $55^\circ$ . When embedded in a lipid bilayer, the DCD oligomer will probably take a tilt angle within this range, and we expect the above trend hold. If the tilt angle further increases, for example in the transition to the membrane surface-parallel orientation, the trend may be changed.

The embedding of the DCD oligomer in lipid bilayers strongly influences the bilayers. Unlike most of the membrane proteins that are sitting in the membranes with the structural axis perpendicular to the membrane surface and has a symmetry effect on the membrane around this axis, the tilted orientation does not introduce a

symmetric effect around its axis to the lipid bilayers. As shown in Fig. 6, the influence on the lipid bilayer is not symmetric around the z-axis. Instead, the distorted bilayer has an inversion center. Both CG and atomistic simulations showed the same feature. The distortion mainly involves a bending and thinning of the membrane around the interface between the DCD oligomer and the bilayers. This is caused by the inward moving of the lipid head groups towards the bilayer center along the hydrophilic gap on the outer surface of the DCD oligomer. This inward motion of the lipid head groups also exposes the side opening of the DCD oligomer to the water solution, which can facilitate the ion permeation. Therefore, this unique distortion of the lipid bilayer clears the major ion permeation pathway and makes the ion permeation more efficient.

From our results, we conclude that the composition of the membrane has a significant impact on the orientation and activity of the DCD oligomer. Basically, the thicker the bilayer, the smaller the tilt; and the smaller the tilt, the smaller the conductance. The addition of cholesterol makes the membranes thicker, and leads to a lower conductance. However, we should keep in mind that cell membranes are much more complex than the simplified models we used for our study, and we have not studied the oligomerization and insertion of the DCD in membranes, so we cannot conclude the selectivity mechanism of the DCD against bacteria from these data alone. Rather, our work revealed the relation of the membrane thickness and the orientation and conductance of the DCD oligomer after embedded into the membrane. Since the conductance of the DCD oligomer is highly related to its activity, we think the activity of DCD is closely related to the membrane composition after forming pores in the membrane. To reveal the full selectivity mechanism, more realistic membrane models and the pore formation processes should be studied in the future.

## **AUTHOR CONTRIBUTIONS**

CS designed and performed the research. BLdG and MSPS supervised the research. CS, BLdG and MSPS wrote the manuscript.

## **ACKNOWLEDGMENTS**

We thank Dr Phillip J. Stansfeld for advice with CG simulations, and Dr Matthieu Chavent for advice on visualization. The research was supported by a Marie Curie Intra European Fellowship within the 7th European Community Framework Programme (CS and MSPS). Research in MSPS's group is supported by the BBSRC, EPSRC, Leverhulme Trust, and Wellcome. CS is supported by grants from the Ministry of Science and Technology of China (National Key R&D Program of China, 2016YFA0500401), National Natural Science Foundation of China (Grant Number 21873006), and the Young Thousand Talents Program of China. BLdG acknowledges funding from the German Research Foundation DFG via SFB803 (project A03).

## References

1. Ventola, C.L. 2015. The Antibiotic Resistance Crisis: Part 1: Causes and Threats. *Pharm. Ther.* 40: 277–283.
2. Hancock, R.E.W., and H.-G. Sahl. 2006. Antimicrobial and host-defense peptides as new anti-infective therapeutic strategies. *Nat. Biotechnol.* 24: 1551–1557.
3. Brogden, K.A. 2005. Antimicrobial peptides: pore formers or metabolic inhibitors in bacteria? *Nat. Rev. Microbiol.* 3: 238–250.
4. Zasloff, M. 2002. Antimicrobial peptides of multicellular organisms. *Nature.* 415: 389–395.
5. Bennett, W.F.D., C.K. Hong, Y. Wang, and D.P. Tieleman. 2016. Antimicrobial Peptide Simulations and the Influence of Force Field on the Free Energy for Pore Formation in Lipid Bilayers. *J. Chem. Theory Comput.* 12: 4524–4533.
6. Mihajlovic, M., and T. Lazaridis. 2010. Antimicrobial peptides in toroidal and cylindrical pores. *Biochim. Biophys. Acta - Biomembr.* 1798: 1485–1493.
7. Thøgersen, L., B. Schiøtt, T. Vosegaard, N.C. Nielsen, and E. Tajkhorshid. 2008. Peptide Aggregation and Pore Formation in a Lipid Bilayer: A Combined Coarse-Grained and All Atom Molecular Dynamics Study. *Biophys. J.* 95: 4337–4347.
8. Wang, Y., C.H. Chen, D. Hu, M.B. Ulmschneider, and J.P. Ulmschneider. 2016. Spontaneous formation of structurally diverse membrane channel architectures from a single antimicrobial peptide. *Nat. Commun.* 7: 13535–13535.
9. Wang, Y., D.E. Schlamadinger, J.E. Kim, and J.A. McCammon. 2012. Comparative molecular dynamics simulations of the antimicrobial peptide CM15 in model lipid bilayers. *Biochim. Biophys. Acta BBA - Biomembr.* 1818: 1402–1409.
10. Parton, D.L., E.V. Akhmatkaya, and M.S.P. Sansom. 2012. Multiscale simulations of the antimicrobial peptide maculatin 1.1: Water permeation through disordered aggregates. *J. Phys. Chem. B.* 116: 8485–8493.
11. Pino-Angeles, A., J.M. Leveritt, and T. Lazaridis. 2016. Pore Structure and Synergy in Antimicrobial Peptides of the Magainin Family. *PLoS Comput. Biol.* 12: 1–17.
12. Cirac, A.D., G. Moiset, J.T. Mika, A. Koçer, P. Salvador, B. Poolman, S.J. Marrink, and D. Sengupta. 2011. The molecular basis for antimicrobial activity of pore-forming cyclic peptides. *Biophys. J.* 100: 2422–2431.
13. Leontiadou, H., A.E. Mark, and S.J. Marrink. 2006. Antimicrobial peptides in action. *J. Am. Chem. Soc.* 128: 12156–61.
14. Giuliani, A., G. Pirri, and S. Nicoletto. 2007. Antimicrobial peptides: an overview of a promising class of therapeutics. .
15. Aoki, W., and M. Ueda. 2013. Characterization of antimicrobial peptides toward the development of novel antibiotics. *Pharmaceuticals.* 6: 1055–1081.

16. Midura-Nowaczek, K., and A. Markowska. 2014. Antimicrobial peptides and their analogs: Searching for new potential therapeutics. *Perspect. Med. Chem.* 6: 73–80.
17. Oyston, P.C.F., M.A. Fox, S.J. Richards, and G.C. Clark. 2009. Novel peptide therapeutics for treatment of infections. *J. Med. Microbiol.* 58: 977–987.
18. Schitteck, B., R. Hipfel, B. Sauer, J. Bauer, H. Kalbacher, S. Stevanovic, M. Schirle, K. Schroeder, N. Blin, F. Meier, G. Rassner, and C. Garbe. 2001. Dermcidin: a novel human antibiotic peptide secreted by sweat glands. *Nat. Immunol.* 2: 1133–1137.
19. Rieg, S., H. Steffen, S. Seeber, A. Humeny, H. Kalbacher, K. Dietz, C. Garbe, and B. Schitteck. 2005. Deficiency of dermcidin-derived antimicrobial peptides in sweat of patients with atopic dermatitis correlates with an impaired innate defense of human skin in vivo. *J Immunol.* 174: 8003–8003.
20. Rieg, S., C. Garbe, B. Sauer, H. Kalbacher, and B. Schitteck. 2004. Dermcidin is constitutively produced by eccrine sweat glands and is not induced in epidermal cells under inflammatory skin conditions. *Br J Dermatol.* 151: 534–539.
21. Lai, Y.-P., Y.-F. Peng, Y. Zuo, J. Li, J. Huang, L.-F. Wang, and Z.-R. Wu. 2005. Functional and structural characterization of recombinant dermcidin-1L, a human antimicrobial peptide. *Biochem. Biophys. Res. Commun.* 328: 243–50.
22. Rieg, S., S. Seeber, H. Steffen, A. Humeny, H. Kalbacher, S. Stevanovic, A. Kimura, C. Garbe, and B. Schitteck. 2006. Generation of multiple stable dermcidin-derived antimicrobial peptides in sweat of different body sites. *J. Invest. Dermatol.* 126: 354–65.
23. Senyürek, I., M. Paulmann, T. Sinnberg, H. Kalbacher, M. Deeg, T. Gutschmann, M. Hermes, T. Kohler, F. Götz, C. Wolz, A. Peschel, and B. Schitteck. 2009. Dermcidin-derived peptides show a different mode of action than the cathelicidin LL-37 against *Staphylococcus aureus*. *Antimicrob. Agents Chemother.* 53: 2499–509.
24. Senyürek, I., G. Döring, H. Kalbacher, M. Deeg, a Peschel, C. Wolz, and B. Schitteck. 2009. Resistance to dermcidin-derived peptides is independent of bacterial protease activity. *Int. J. Antimicrob. Agents.* 34: 86–90.
25. Niyonsaba, F., a Suzuki, H. Ushio, I. Nagaoka, H. Ogawa, and K. Okumura. 2009. The human antimicrobial peptide dermcidin activates normal human keratinocytes. *Br. J. Dermatol.* 160: 243–9.
26. Jung, H.H., S.-T. Yang, J.-Y. Sim, S. Lee, J.Y. Lee, H.H. Kim, S.Y. Shin, and J.I. Kim. 2010. Analysis of the solution structure of the human antibiotic peptide dermcidin and its interaction with phospholipid vesicles. *BMB Rep.* 43: 362–368.
27. Melo, M.N., R. Ferre, and M. a R.B. Castanho. 2009. Antimicrobial peptides: linking partition, activity and high membrane-bound concentrations. *Nat. Rev. Microbiol.* 7: 245–250.
28. Song, C., C. Weichbrodt, E.S. Salnikov, M. Dynowski, B.O. Forsberg, B. Bechinger, C. Steinem, B.L. de Groot, U. Zachariae, and K. Zeth. 2013. Crystal structure and functional mechanism of a human antimicrobial membrane channel. *Proc. Natl. Acad. Sci. U. S. A.* 110: 4586–91.
29. Marrink, S.J., and D.P. Tieleman. 2013. Perspective on the Martini model. *Chem. Soc. Rev.* 42: 6801–6822.
30. Hess, B., C. Kutzner, D. van der Spoel, and E. Lindahl. 2008. GROMACS 4: Algorithms for Highly Efficient, Load-Balanced, and Scalable Molecular Simulation. *J. Chem. Theory Comput.* 4: 435–447.

31. Marrink, S.J., H.J. Risselada, S. Yefimov, D.P. Tieleman, and A.H. De Vries. 2007. The MARTINI force field: Coarse grained model for biomolecular simulations. *J. Phys. Chem. B.* 111: 7812–7824.
32. Berendsen, C., P.M. Postma, W.F.V. Gunsteren, A. DiNola, R. Haak, I. Introduction, H.J.C. Berendsen, J.P.M. Postma, W.F. van Gunsteren, and J.R. Haak. 1984. Molecular dynamics with coupling to an external bath. *J. Chem. Phys.* 81: 3684–3690.
33. Bussi, G., D. Donadio, and M. Parrinello. 2007. Canonical sampling through velocity rescaling. *J. Chem. Phys.* 126: 014101–014101.
34. Stansfeld, P.J., J.E. Goose, M. Caffrey, E.P. Carpenter, J.L. Parker, S. Newstead, and M.S.P. Sansom. 2015. MemProtMD: Automated Insertion of Membrane Protein Structures into Explicit Lipid Membranes. *Structure.* 23: 1350–1361.
35. Kutzner, C., H. Grubmüller, B.L. de Groot, and U. Zachariae. 2011. Computational Electrophysiology : the Molecular Dynamics of Ion Channel Permeation and Selectivity in Atomistic Detail. *Biophys. J.* 101: 1–9.
36. Kutzner, C., D. Köpfer, J.-P. Machtens, B.L. de Groot, C. Song, and U. Zachariae. 2016. Insights into the function of ion channels by computational electrophysiology simulations. *Biochim. Biophys. Acta BBA - Biomembr.* 1858: 1741–1752.
37. Klauda, J.B., R.M. Venable, J.A. Freites, J.W. O'Connor, D.J. Tobias, C. Mondragon-Ramirez, I. Vorobyov, A.D. MacKerell, and R.W. Pastor. 2010. Update of the CHARMM all-atom additive force field for lipids: validation on six lipid types. *J. Phys. Chem. B.* 114: 7830–7843.
38. Wolf, M.G.M.M.G.M.G., M. Hoefling, C. Aponte-santamaría, H. Grubmüller, and G. Groenhof. 2010. g\_membed: Efficient insertion of a membrane protein into an equilibrated lipid bilayer with minimal perturbation. *J. Comput. Chem.* 31: 2169–2174.
39. Jo, S., T. Kim, V.G. Iyer, and W. Im. 2008. CHARMM-GUI: A web-based graphical user interface for CHARMM. *J. Comput. Chem.* 29: 1859–1865.
40. Parrinello, M., and a. Rahman. 1981. Polymorphic Transitions in Single Crystals: a New Molecular Dynamics Method. *J Appl Phys.* 52: 7182–7190.
41. Nosé, S., and M.L. Klein. 1983. Constant pressure molecular dynamics for molecular systems. *Mol. Phys.* 50: 1055–1076.
42. Nosé, S.S. 1984. A molecular dynamics method for simulations in the canonical ensemble. *Mol. Phys.* 52: 255–268.
43. Hoover, W.G. 1985. Canonical dynamics: Equilibrium phase-space distributions. *Phys. Rev. A.* 31: 1695–1697.
44. Darden, T., D. York, and L. Pedersen. 1993. Particle mesh Ewald: An Nlog(N) method for Ewald sums in large systems. *J Chem Phys.* 98: 10089–10092.
45. Essmann, U., L. Perera, M.L. Berkowitz, T. Darden, H. Lee, and L.G. Pedersen. 1995. A smooth particle mesh Ewald method. *J Chem Phys.* 103: 8577–8593.
46. Matsuzaki, K. 1999. Why and how are peptide-lipid interactions utilized for self-defense? Magainins and tachyplesins as archetypes. *Biochim. Biophys. Acta - Biomembr.* 1462: 1–10.

47. Chimere, C., L. Movileanu, S. Pezeshki, M. Winterhalter, and U. Kleinekathöfer. 2008. Transport at the nanoscale: Temperature dependence of ion conductance. *Eur. Biophys. J.* 38: 121–125.
48. Kuyucak, S., and S.H. Chung. 1994. Temperature dependence of conductivity in electrolyte solutions and ionic channels of biological membranes. *Biophys. Chem.* 52: 15–24.

## Figures

*Figure 1:* Coarse grained (CG) self-assembly simulations of DCD/lipid bilayer systems, and the atomistic computational electrophysiology (CE) simulation system. **A & B** show two initial systems for the CG simulations, with the helix bundle (green-cyan) perpendicular or parallel respectively to the plane of the initial slab contacting lipid molecules (dark grey). **C & D** show two possible resultant orientations of the DCD oligomer relative to the self-assembled bilayer (lipid phosphate particles only are shown in dark grey) at the end of the 0.5  $\mu$ s CG simulations. The tilt angle is indicated by  $\theta$  in the panel **C**. The small transparent light-blue spheres are water particles. **E** The atomistic computational electrophysiology (CE) simulation system, where the green-cyan cartoons represent the DCD oligomer, the grey spheres are the P atoms of the lipid (DMPC) head groups and the red and blue spheres are  $\text{Cl}^-$  and  $\text{Na}^+$  ions respectively. W1 and W2 represent the two aqueous compartments between which a voltage difference of ~250-450 mV was maintained in the CE simulations.

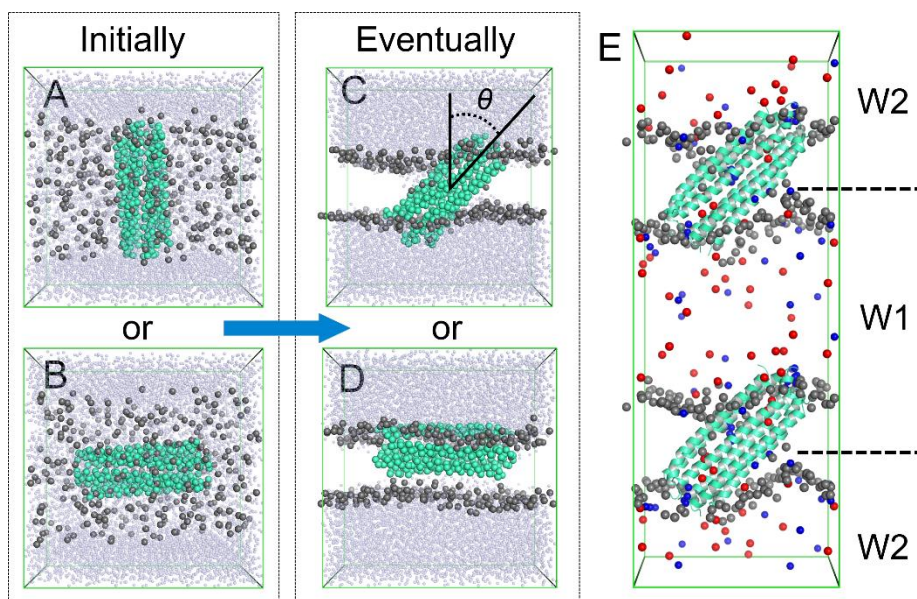
*Figure 2:* DCD helix bundle tilt angle evolution CG simulations in the presence of DMPC (upper row), DPPC (middle row) or DSPC (lower row) lipids, with 0%, 20% and 40% cholesterol. The red lines correspond to simulations with the DCD oligomer axis initially parallel to the z-axis (see Fig. 1A), while the blue lines correspond to simulations with the DCD oligomer initially perpendicular to the z-axis (see Fig. 1B). For each case, ten independent simulations of 0.5  $\mu$ s duration were performed.

*Figure 3:* Mean tilt angles of the DCD helix bundle relative to the bilayer normal in lipid bilayers with different thicknesses. The red, black and blue dashed lines represent the simulation results with DMPC, DPPC and DSPC lipid bilayers respectively. The circle, square and triangle symbols represent the simulations with 0%, 20% and 40% cholesterol respectively. The standard errors of the means of the tilt angles and membrane thicknesses for each case are smaller than or comparable to the size of the symbols, so they are not shown here for clarity. Please refer to the SI for more detailed data.

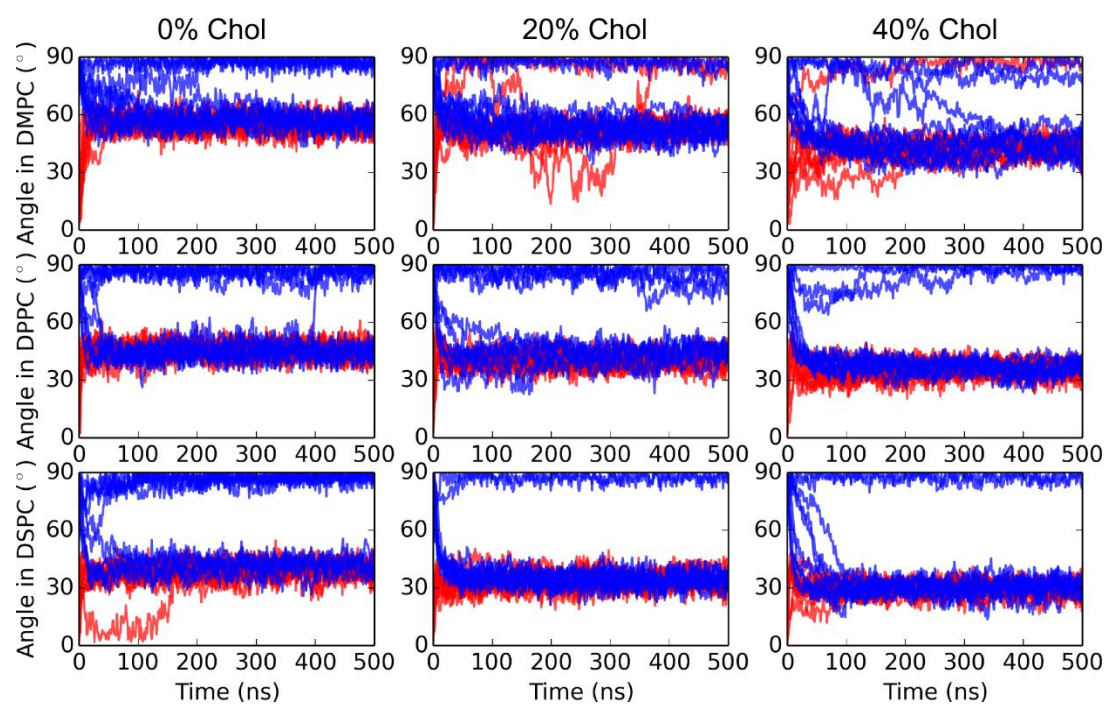
Figure 4: Tilt angle evolution of the DCD oligomer in DMPC (red), DPPC (black) and DSPC (blue) bilayers as observed in the atomistic simulations. **A** The tilt angle evolution in the single-layer simulations, with the initial channel axis normal to the bilayer surface, and **B** the tilt angle evolution in the double-layer simulations, where the initial configurations were taken from the single-layer simulations at 200 ns for DMPC and DSPC, and at 400 ns for DPPC, as shown in **A**. The solid and dashed lines in **B** represent the two channels in the two bilayers of the double-patch CE systems respectively.

Figure 5: Correlation between the average single channel conductance as estimated by CE simulations and the corresponding tilt angle of the DCD oligomer. Each scatter was obtained from a 200-ns atomistic molecular dynamics simulation under a transmembrane potential of ~250-450 mV as described in the method section. The blue circles were derived from the CE simulations with DMPC, DPPC or DSPC, and denoted as D[MPS]C. The black circles were obtained from the CE simulations with DMPC and cholesterol (DMPC:CHOL=8:2). The red plots were derived from our previous simulations of DCD in a bilayer composed of POPE:POPG (3:1) at 310 K (28). As previous studies showed that the conductance of ion channels at 345 K is less than twice of that at 310 K (47, 48), we simply doubled the conductance of DCD in POPE and POPG at 310 K (empty squares) to roughly estimate the conductance at 345 K (red squares). The Pearson correlation coefficient was 0.65 based on the calculations for the results at 345 K. For the detailed data including the error estimation, please refer to Table S5.

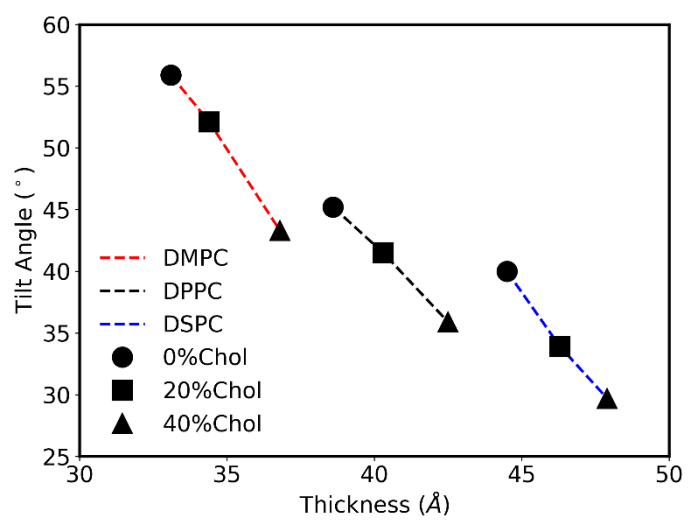
Figure 6: The local DMPC bilayer thickness around the DCD helix bundle from **A** CG and **B** atomistic MD simulations. The green-cyan spheres/cartoons represent the DCD oligomer. The blue, white and red spheres represent the average local bilayer thickness averaged across a trajectory. The bilayer thickness was calculated by the distance between the phosphate particles (or P atoms) of the two leaflets with our in-house analysis tool.



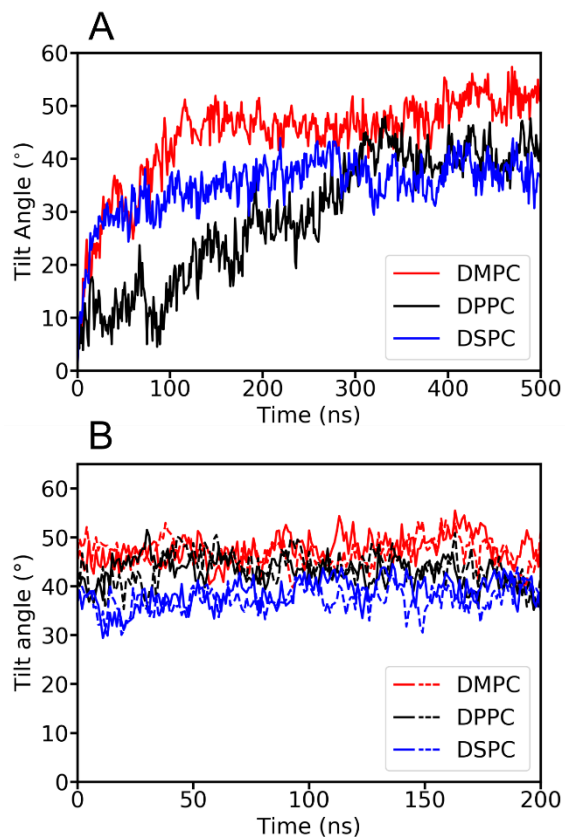
Song et al., Fig. 2



Song et al., Fig. 3



Song et al., Fig. 4



Song et al., Fig. 5

